From Mesoscale Back to Atomistic Models: A Fast Reverse-Mapping Procedure for Vinyl Polymer Chains

Giuseppe Santangelo,[§] Andrea Di Matteo,[§] Florian Müller-Plathe,[†] and Giuseppe Milano*[,‡]

STMicroelectronics c/o IMAST P.le Enrico Fermi, 1 Località Granatello I-80055 Italy, Eduard-Zintl-Institut für Anorganische und Physikalische Chemie, Technische Universität Darmstadt, Petersenstrasse 20, D-64287 Darmstadt, Germany, and Dipartimento di Chimica, Università di Salerno, I-84084 via Ponte don Melillo Fisciano (SA), Italy

Received: September 22, 2006; In Final Form: January 17, 2007

This paper introduces a systematic procedure to obtain well-relaxed atomistic melt structures from mesocale models of vinyl polymers based on sequences of diads. Following the methodology introduced by Milano and Müller-Plathe [*J. Phys. Chem. B.* **2005**, 109, 18609], coarse-grain models consisting of sequences of superatoms of two different types meso and racemo have been used to relax mesocale melts of atactic and syndiotactic polystyrene. The proposed method, based on a fully geometrical approach, does not involve expensive potential energy and force evaluations and allows a very fast and efficient reconstruction of the atomistic detail. The method, successfully tested against experimental data, allows us to obtain all atom models of both stereoregular and stereoirregular polymers and opens the possibility of relaxing large molecular weight melts of vinyl chains.

1. Introduction

A computational investigation of the structure−property relations for polymeric materials necessitates the preparation of equilibrated melts of long, entangled chains. Melts consisting of oligomers can be equilibrated by sufficiently long molecular dynamics or Monte Carlo simulations. High molecular weight polymer chains are very difficult to treat because they are hard to relax. Although computational power increases 10-fold every 5 years, the huge number of degrees of freedom and the large relaxation times typical of an entangled polymer melt effectively precludes fully atomistic approaches to the investigation of long polymer chains. Just to have an idea, the longest relaxation of an entangled polymer melt of length N scales at least as N^3, giving at least N^4 in CPU time and the required computer time for a reliable equilibration is out of reach.

Polymer coarse-grained models have been widely utilized in order to solve this problem.[1−6] The general strategy is to reduce the number of the degrees of freedom by simplifying the models and keeping only those degrees of freedom that are relevant for a particular range of interest. In general, the price to pay for a coarser model is the loss of chemical detail. Recently, to obtain realistic coarse-grain polymer models, methods to map automatically atomistic features to mesoscopic models have been proposed.[7−11] This approach allows us to speed up the simulations but retaining information of the underlying chemical structure.

To this purpose, several atoms are grouped together into "super-atoms", the typical super-atom is comprised of on the order of ten atoms. The potentials between super-atoms are adjusted to reproduce mainly structural properties of the polymer. The structure of an ensemble of polymer chains are described by the distributions of geometrical quantities. These distributions are extracted from atomistic simulations of oligomers and can be used as targets to be reproduced by the coarse-grained model.

Following this approach, different polymer properties have been calculated by mesoscale simulations in good agreement with experimental data.[9−12]

In the case of vinyl polymers and in particular for polystyrene, due to its industrial relevance, different coarse-grain models have been recently proposed. The application of different mapping schemes to coarse-grain polystyrene and the related results are good illustrations of the idea that, for a given polymer, the choice of the mapping scheme is not unique, and the adopted coarse-graining strategy is related mainly to the purpose of the coarse-grained simulation.

Some of us introduced a systematic procedure, based on atomistic simulations of polystyrene oligomers (10-mers) using iterative Boltzmann inversion, to coarse-grain atomistic models of vinyl polymers into a mesoscopic model, which is able to keep information about chain tacticity.[13] The model consists of chains of superatoms centered on methylene carbons of two different types according to the kind of diad (m or r) they belong to. The change to a coarse-grained scale leads to an effective speed-up of 2000 for the computational efficiency of the relaxation of the chains. The proposed mesoscale model has been successfully tested against structural and dynamical properties of the melt for different chain lengths for atactic polystyrene as well as for stereoregular chains and opened the possibility of relaxing melts of high molecular weight vinyl polymers.[13] Sun and Faller reported a coarse-grain model of polystyrene based on iterative Boltzmann inversion to study the dynamics of melts.[14] They further extended this approach to polystyrene−polyisoprene blends.[15] Very recently, Kremer and co-workers introduced a coarse-grain model of polystyrene based on atomistic simulations of isolated polystyrene dimers where

* Corresponding author phone: +39 089 96 9567; fax: +39 089 96 9602; e-mail: gmilano@unisa.it.
† Technische Universität Darmstadt.
‡ Università di Salerno.
§ STMicroelectronics.

10.1021/jp066212l CCC: $37.00
Published on Web 02/24/2007

the bonded parameters are chosen in a way which takes into account polymer stereochemistry.[16]

The main purpose of this contribution is the development and validation of a reverse mapping procedure suitable for the coarse-grained model based on diads. It generates well-relaxed amorphous vinyl polymers melts structures at the atomistic level starting from the mesoscale models. This is one of the important uses of coarse grained models.[17] In fact, the apparently complicated procedure of *atomistic simulations → derivation of a coarse-grained model; coarse-grained simulations → reverse-mapping and local relaxation of the atomistic model* is an efficient way to obtain well-relaxed polymer structures. After threading an atomistic model through the coarse-grained chains followed by local relaxation of molecular dynamics, atomistic properties, which depend on the behavior of individual atoms, can be calculated.

This paper is organized as follows: section 2 will guide the reader to the earlier work that is essential for understanding the present investigation. In section 3, technical details of both coarse-grained and atomistic simulations are reported. The proposed reverse-mapping strategy and the approach for the reinsertion of atomistic degrees of freedom are reported in sections 4.1 and 4.2. The validation of the method by calculated structural properties of relaxed atomistic models including radial distribution functions, analysis of conformations and structure factors compared with available experimental data is described in section 5.

2. Mesocale Models for Vinyl Polymers

The present section is intended to guide the reader quickly to the earlier work that is essential for understanding the present investigation. Further details and extensive validations of the mesoscale approach can be found in refs 13 and 18.

Vinyl chains present along their backbone sequences of methylene (CH_2) and pseudoasymmetric methyne groups (−CHR). Due to the presence of these pseudoasymmetric carbons, vinyl polymers can be stereoregular or stereoirregular.

The definition of isotactic, syndiotactic, and atactic vinyl polymers are well-established in terms of succession of meso (*m*) and racemo (*r*) diads, so they have been officially adopted as the IUPAC standard. According to the IUPAC stereochemical definitions and notations relating to polymers:[19] "stereoregular vinyl polymers can be defined in terms of the regular sequences of diads; thus an isotactic vinyl polymer consists entirely of *m* diads, i.e., it corresponds to the following succession of relative configuration -*m m m m m m*-, whereas a syndiotactic vinyl polymer consists entirely of *r* diads, corresponding to the sequence -*r r r r r r*-". As for an atactic polymer, it is "A regular polymer, the molecules of which have equal numbers of the possible configurational base units in a random sequence distribution"; i.e. it corresponds to a random sequence of *m* and *r* diads.

A diad can be considered as the shortest distinguishing piece of a stereosequence if two consecutive configurations have the same absolute configuration (e.g., *RR* or *SS*), the diad is meso (*m* diad, see Figure 1a); if they are different (e.g., *RS* or *SR*), the diad is designated as racemo (*r* diad, see Figure 1a).

The basic idea of the coarse-graining scheme is to consider a configurational base unit, in particular a diad, as superatom at the mesoscale level. According to this choice, as depicted in Figure 1b, the center of a superatom is the methylene carbon.

The forcefield corresponding to this choice of mesoscale model has two types of particles *m* or *r*, and three different bond types corresponding to the three indistinguishable triads

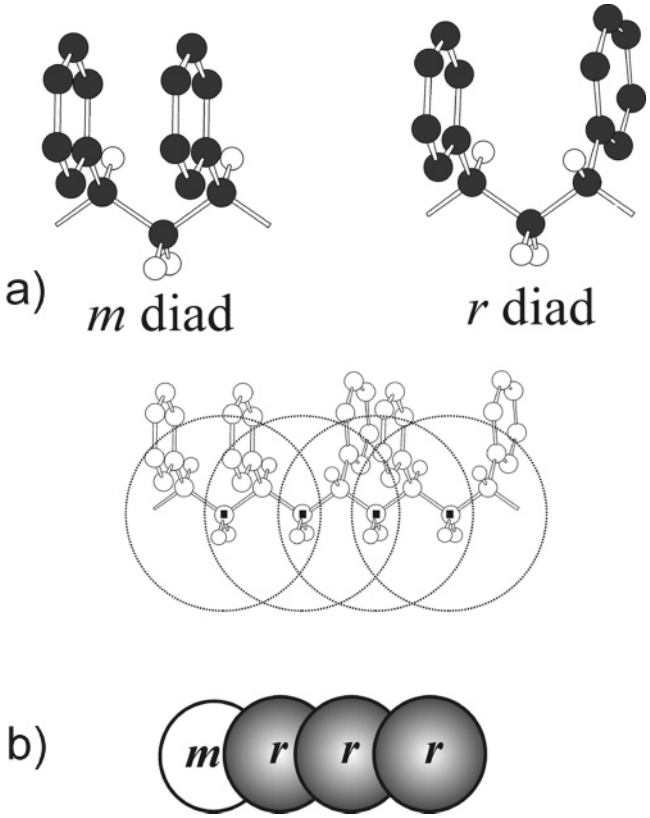

Figure 1. (a) Polystyrene m and r diads in transplanar conformation (hydrogen atoms on phenyl rings are omitted for clarity). (b) Illustration of the mapping scheme for polystyrene:one bead corresponds to a diadic m or r unit. The center of these super-atoms, as indicated by filled squares, are the methylene carbons. In both Figure 1a and b hydrogen atoms on the phenyl ring carbons are not shown for clarity.

(*mm*, *mr*, *rr*), and six angle types corresponding to the six undistinguishable tetrads (*mmm*, *mmr*, *mrm*, *mrr*, *rmr*, *rrr*). Bonds and angle distributions and intermolecular radial distribution functions between the diads extracted from atomistic simulation are considered as target distributions. A valid mesoscale model of a vinyl polymer will produce distributions close to the target ones.

In particular, in the case of polystyrene,[13] the mesoscale model, which reproduces bond and angle distributions as well as intermolecular radial distribution functions almost identical to the target atomistic ones, gives a very good reproduction of experimental structural data.

The parametrization procedure together with mesoscale force field are briefly described in section 3 (Computational Methods), for more detailed information the reader is refererred to refs 13 and 18.

To obtain atomistic structures from the mesoscale models, we considered three different systems. First, an atactic polystyrene melt with chains of the same molecular weight as those used to parametrize the mesoscale force field (56 chains of a-PS decamer, i.e., nine diads) but with a much larger number of chains (150 chains of a-PS decamer). Second, an atactic polysterene melt with large molecular weight chains (three chains of a-PS 351-mer). Third, a syndiotactic polysterene melt with large molecular weight chains (three chains of a-PS 351-mer). Simulations of syndiotactic polystyrene melts have been performed including a numerical torsional potential obtained by iterative Boltzmann inversion of the *rrrr* distribution. In this case, in agreement with experimental findings, the calculated characteristic ratio (∼9) becomes higher than the one of the

TABLE 1: Nonbonded Paramers for Polystyrene

$$(r_{ij}) = 4\epsilon\,[(\sigma/r_{ij})^{12} - (\sigma/r_{ij})^{6}] + q_i q_j /4\pi\epsilon_0 r_{ij}$$

nonbonded interactions[a,b]	ϵ/kJ mol^{-1}	σ/nm	q/e
C_{ali}	0.3519	0.3207	0
H_{ali}	0.318	0.2318	0
C_{aro}	0.294	0.355	−0.115[c]
H_{aro}	0.126	0.242	+0.115
X[d]	0.0100	0.450	0

[a] Nonbonded interactions are excluded between first and second neighbors. [b] The subscripts ali and aro denote aliphatic and aromatic atoms, respectively. In addition, nonbonded interactions between all atoms of a phenyl group are excluded. [c] The charge on carbon 1 of the phenyl group is 0. [d] Phenyl centroid used in the preparatory stage.

corresponding atactic chain. However, although we have this agreement, we want to stress that, in principle, the model used in our preliminary simulations has been derived from stereoregular sequences in an atactic polymer. A correct coarse-grained model for pure syndiotactic polystyrene will probably be different.

Starting from the configurations obtained from the mesocale simulations of the three systems described above, using the procedures described in section 4, the three corresponding all atom models have been obtained and validated against experimental structural data.

3. Computational Methods

3.1. Technical Details of Atomistic Simulations. The molecular dynamics package GROMACS[20,21] was used to run the all-atom simulations under constant volume or constant pressure (Berendsen manostat with coupling time $\tau_p = 2$ ps) and constant temperature (Berendsen thermostat[22] with $\tau_T = 0.2$ ps at a time step of 2 fs). All bond lengths were kept rigid by the SHAKE procedure. The cutoff for nonbonded interactions was $r_c = 1.1$ nm with a Verlet neighbor list[23] cutoff of 1.2 nm. The polystyrene force field has been used already to describe different polystyrene based materials: polystyrene gels,[24,25] amorphous PS calculation of positronium annihilation spectra,[26] anisotropy of diffusion of helium and CO_2 in a nanoporous crystalline phase of syndiotactic PS (s-PS).[27] Details about the forcefield and parameters can be found in Tables 1 and 2.

3.2. Mesoscale Potentials and Force Field Parametrization. Mesoscale potentials obtained by Boltzmann inversion of a multi-peaked distribution approximated by a sum of several Gaussian functions have been recently proposed as a valid alternative to a fully numerical approach for bond and angle terms in mesoscale force-field for polymers:[18]

If we define a Gaussian distribution of a bond length or bond angle denoted as θ, $g_i(\theta) = A_i/w_i\sqrt{\pi/2}\,\exp^{-2\,(\theta-\theta_{ci})^2/w^2 i}$, the mesoscale potential can be obtained by Boltzmann-inverting a sum of such Gaussian distributions:

$$V(\theta) = -kT \ln \sum_{i=1}^{n} g_i(\theta) \tag{1}$$

and the corresponding force:

$$F(\theta) = -4kT \frac{\sum_{i=1}^{n} g_i(\theta) \dfrac{(\theta - \theta_{ci})}{w_i^2}}{\sum_{i=1}^{n} g_i(\theta)} \tag{2}$$

TABLE 2: Bonded Parameters for Polystyrene

bond constraint	distance/nm
C_{ali}-C_{ali}	0.153
C_{ali}-H_{ali}	0.110
C_{aro}-C_{aro}	0.139
C_{aro}-H_{aro}	0.108
C_{ali}-C_{aro}	0.151
C_{aro}-X[a]	0.139

$$V(\phi) = (k_\phi/2)(\phi - \phi_0)^2$$

bond angles	ϕ_0 /deg	K_ϕ /kJ mol^{-1}rad^{-2}
H-C_{ali}-H	109.45	306.4
C_{ali}-C_{ali}-H	109.45	366.9
C_{ali}-C_{ali}-C_{ali}	109.45	482.3
C_{aro}-C_{ali}-H	109.45	366.9
C_{ali}-C_{ali}-C_{aro}	109.45	482.3
C_{ali}-C_{aro}-C_{aro}	120.0	376.6
C_{aro}-C_{aro}-C_{aro}	120.0	376.6
C_{aro}-C_{aro}-H	120.0	418.8

$$V(\tau) = (k_\tau/2)[1 - \cos 3(\tau - \tau_0)],\ cis \text{ at } 0°$$

dihedral angles	τ_0/deg	k_τ/kJ mol^{-1}
C_{ali}-C_{ali}-C_{ali}-C_{ali}	180.0	12.0
C_{ali}-C_{ali}-C_{ali}-H(terminal methyl)	180.0	12.0

$$V(\delta) = (k_\delta/2)(\delta - \delta_0)^2,\ cis \text{ at } 0°$$

harmonic dihedral angles	δ_0 /deg	K_δ /kJ mol^{-1}rad^{-2}
C_{aro}-C_{aro}-C_{aro}-C_{aro}	0.0	167.4
$C2_{aro}$-$C3_{aro}$-$C1_{aro}$-H[on *C2*]	0.0	167.4
$C2_{aro}$-$C3_{aro}$-$C1_{aro}$-C_{ali}[on *C2*]	0.0	167.4

[a] Phenyl centroid used in the preparatory stage, bonded with carbon C1 and C4 of phenyl ring (see Scheme 1a).

Additional information about the multicentred Gaussian-based potentials (MG-potentials) employed here can be found in refs 13 and 18.

As for the nonbonded part of the potential, pressure-corrected CG numerical potential optimized by iterative Boltzmann inversion have been used.[28] The effective nonbonded potential $V(r)$ is derived from a given tabulated starting potential $V_0(r)$, targeting to match the radial distribution function $g(r)$.

The potential is iteratively improved by successive corrections,

$$V_{j+1}(r) = V_j(r) + kT \ln \frac{g_j(r)}{g_{t\,\mathrm{arg}\,et}(r)} \tag{3}$$

Further details of the parametrization procedure, including a complete set of distribution plots, and its validation against structural and dynamical properties can be found in ref 13.

3.3. Technical Details of Coarse Grained Simulations. For CG simulations, the GMQ_num code,[29] a version of the GMQ package[30] able to handle numerical potentials and modified in order to implement multicentred Gaussian potentials (see mesoscale potential section), was used. The bulk simulations were performed at constant temperature (500 K) and constant pressure ($P = 1$ bar) for production runs. The time constants for the loose coupling thermostat and manostat were set to 0.1 and 5 ps. A time step of 15 fs was used. Nonbonded interactions were truncated beyond 15 Å.

4. Reverse Mapping

4.1. Rebuilding the Atomistic Model: Structure Chirality and Dihedral Conformations. The strategy chosen for an efficient reverse-mapping is based on rigid superposition (rotation) of atomistic diads on the coarse-grained coordinates

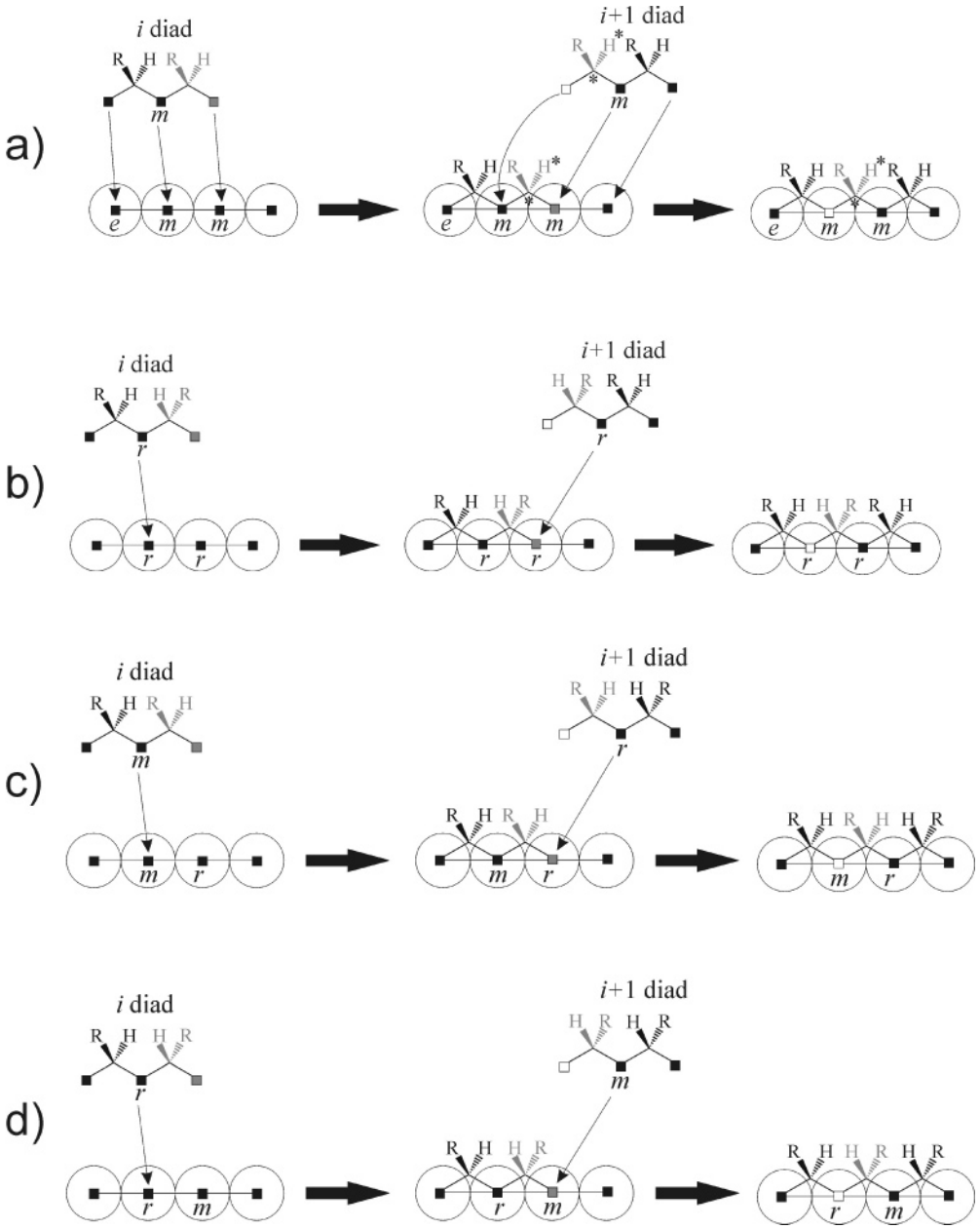

Figure 2. Atomistic diads rebuilding. In the Figure 3 all four possible (a) mm, (b) rr, (c) mr, (d) rr cases are depicted. Depending to the end group absolute R or S configuration each the four possible diad sequence can be translated in the correct atomistic sequence accordind to the mapping rules indicated in Table 3.

obtained from the mesoscale simulations. In particular, as sketched in Figure 2, in a chain made of *i* diads, the atomistic degrees of freedom are rebuilt superposing one by one atomistic diad structures corresponding to different *m* or *r* superatoms.

For a consistent rebuilding of the atomistic polymer structure, great care has to be taken to reinsert diads of proper chirality.

Figure 2a shows the case of an end group, e, followed by a sequence of two m diads. The first inserted structures are the end groups, at the beginning of each chain, with equal probability, an end group of absolute chirality *R* or *S* is chosen. This initial choice of the absolute configuration determines the absolute configuration of the atomistic sequence utilized for the reverse-mapping of the entire chain. For instance, given an *R* chirality of the end group, a sequence of two *m* superatoms is formed by the addition of two diads in which the chiral carbons (indicated with an asterisk in Figure 2a) have both *R* configuration. Given the chirality *S* of the end group the same sequence of two *m* superatoms is translated into an atomistic structure by adding two diads both of *S* configuration. Similar considerations can be done for all possible sequences of diads sketched in Figure 2a−d. Table 3 summarizes, in the form of *mapping rules*, the sequences in terms of absolute chirality that have to be utilized for diad reverse-mapping of a vinyl chain in the two possible *R* or *S* representations (i.e., *R* or *S* end group configuration).

Once the chirality of the end group is fixed, it is possible to establish from the superatoms sequences of the coarse grained model the chirality of all the repeating units that have to be added. Then, the chain reverse-mapping can proceed as indicated in Figure 2a. First, the atomistic end group is rebuilt by superposing the three superatom centers with the corresponding three methylene groups (indicated by filled squares in Figure 2a). In a similar way, the following diad insertion (see diad *i* + 1 in Figure 2a) is done superposing the three methylene groups of the atomistic diad model indicated by squares with their corresponding mesoscale particle centers as indicated in the

TABLE 3: Rules for Diad Reverse-Mapping in the Two Possible R or S Representations of a Vinyl Chain[a]

representation	atomistic diads		chain sequence	representation	atomistic diads		chain sequence
R	***i***	***i*** + 1		S	***i***	***i*** + 1	
mm	RR	RR	RRR	mm	SS	SS	SSS
rr	RS	SR	RSR	rr	SR	RS	SRS
mr	RR	RS	RRS	mr	SS	SR	SSR
rm	RS	SR	RSR	rm	SR	RS	SRS

[a] The pseudo-asymmetric −CHR− groups superimposed in the back-mapped structure have been reported in gray as in Figure 3.

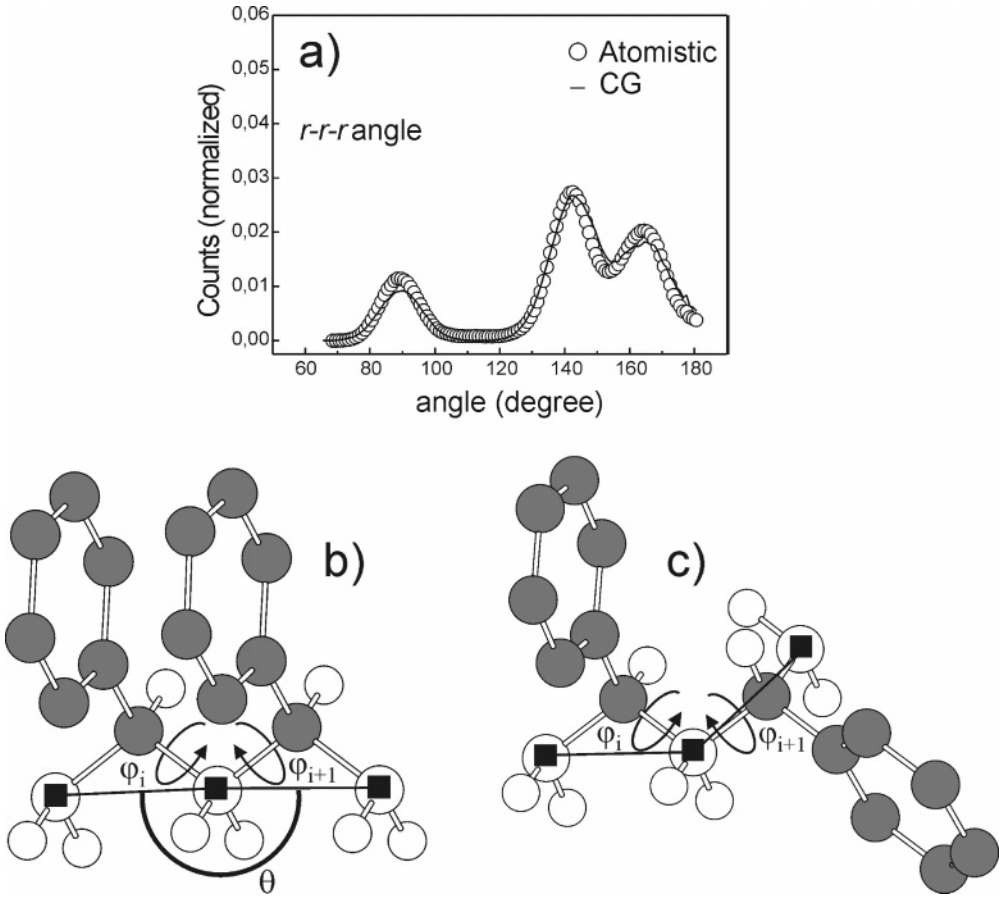

Figure 3. (a) Distribution of r-r-r mesoscale angle. Correspondence between atomistic torsions φ_i and φ_{i+1} around the two backbone bonds of the methylene group and the mesocale angle θ; (b) mesoscale angle $\theta = 180°$ corresponding to an underlying trans trans conformation of the two dihedrals of the atomistic model; (c) mesoscale angle $\theta = 120°$ corresponding to an underlaying trans gauche (or gauche trans) conformation of the two dihedrals of the atomistic model.

Figure 2a. Additional conditions are considered for the superposition of a non end group diad. In particular, in order to have consistent geometries the last chiral carbon of the inserted *i*-diad and the first chiral carbon of the $i + 1$-diad (indicated by an asterisk in Figure 2a) and the hydrogen atoms bonded to these carbons (indicated also by and asterisk in Figure 2a) have to be superimposed.

To have atomistic structures as reliable as possible, further information is obtained from angles between two successive superatoms bonds. The mesoscale angle distribution of Figure 3a (*rrr* angle distribution) shows three peaks, one at about 90° and two more at 120° and 180°. The other four possible *mmm*, *mmr*, *mrm*, *rmr*, and *mrr* distributions (not shown, see ref 13) show analogously at most three peaks in the same positions. The three states of the mesoscale angle ∼90, ∼120, and ∼180° are related to three possible underlying atomistic geometries.

In particular, as shown in Figures 3, the angle between two mesocale bonds is mainly determined by torsions (φ_i and φ_{i+1} in Figure 3b and c) around the two backbone bonds of the methylene group. Figure 3b and c show two cases of mesoscale angles around 180° and 120°. In the first case, the mesoscale angle ($\theta = 180°$, atomistic structure in 3b) corresponds to an underlying trans trans conformation of the two dihedrals of the atomistic model. In the second case, the mesoscale angle ($\theta = 120°$, atomistic structure in 3c) corresponds to an underlying trans gauche (or gauche trans) conformation of the two dihedrals of the atomistic model. Similarly, the mesoscale angle of ∼90° corresponds to a gauche gauche conformation of the two atomistic dihedrals. Then, when a diad *i* is to be inserted according to the angle $(i - 1) - (i) - (i + 1)$, the conformations of the two backbone dihedral angles of the central methylene can be decided. In some cases, several atomistic conformations may correspond to the same mesososcale angle. This is the case when the mesoscale angle is ∼120°, both trans gauche and gauche trans atomistic conformations are compatible and, if the gauche− conformations are also considered, the number is double. In these cases, the atomistic structure is chosen which allows the best superposition in terms of lowest root-mean-square deviation (rmsd) between the atoms.

In summary, from end group absolute chirality, the diad identity (*m* or *r*) and the mesoscale angle, it is possible to decide the chiral carbon configurations and to have a very reasonable

guess of the backbone dihedrals of the atomistic diads that have to be superimposed.

In the practical implementation of the reverse-mapping method proposed here, the atomistic structure is rebuilt for each chain by sequences of successive *n* superpositions starting from one end group (*n* is the number of diads including the end groups). According to the rules above, atomistic diads of different chiralities and different dihedral conformations are selected from a library containing Cartesian coordinates of possible structures. Each atomistic structure in the library is in the minimum energy geometry for the given dihedral conformation of the isolated diad.

4.2. Structure Superposition. As described in the preceding subsection, the reverse-mapping strategy involves a superposition obtained by rigid rotation of atomistic diads on the coarse-grained coordinates. The structures obtained have to minimize the rmsd between methylene carbons and superatom centers and between some of the atoms (first chiral carbon and the hydrogen bonded to it) of the inserted diad with the corresponding atoms (last chiral carbon and the hydrogen bonded to it) of the previously inserted diad. In this subsection, the main features of the superposition method is described.

Structure superposition methods are used widely to compare molecular structures. They allow to superimpose molecular structures to facilitate visual comparisons and to give a quantitative measure of shape similarity as the root-mean-square deviation of distances between corresponding atoms. One can use different numerical and analytical approaches to the rigid fit of two structures. Methods based on linear algebra have been widely employed.[31−33]

In general, the problem can be solved by finding the optimal orthogonal transformation and requires determination of a rotation matrix $\boldsymbol{R}$ and a translation vector that will superimpose two sets of coordinates. In our case, due to the presence of chiral centers, the additional requirement of chirality preservation has to be considered. In linear algebra language, this means that the orthogonal transformation must not include reflections.

Our choice is a method based on quaternions introduced by Kearsley.[34] Which is analytical (i.e., fast) and assures chirality preservation.

Quaternions are a non-commutative extension of complex numbers and are widely used to describe rotations in classical as well as quantum and relativistic physics.[35]

A quaternion is given by

$$q = (q_1, q_2, q_3, q_4) \tag{4}$$

Usually, q_1 can be indicated as real part and $\boldsymbol{q}$ the vector part of the quaternion:

$$q = (q_1, \mathbf{q}) \tag{5}$$

the product of two quaternions is a quaternion and can be expressed using scalar and vector products:

$$pq = (p_1,\mathbf{p})(q_1,\mathbf{q}) = (p_1q_1 - \mathbf{p}\cdot\mathbf{q}, p_1\mathbf{q} + q_1\mathbf{p} + \mathbf{p}\wedge\mathbf{q}) \tag{6}$$

It can be shown that a quaternion can be used as a rotation operator for a vector. The vector can be considered as a quaternion with zero scalar component:

$$(0, \mathbf{r}') = \hat{\mathrm{q}}^{-1}(0, \mathbf{r})\hat{\mathrm{q}} = (0, {q_1}^2\mathbf{r} + (\mathbf{r}\cdot\mathbf{q})\mathbf{q} + 2q_1(\mathbf{r}\wedge\mathbf{q}))$$

$$\mathbf{r}' = \boldsymbol{R}\mathbf{r}$$

$$= \begin{pmatrix} {q_1}^2 + {q_2}^2 - {q_3}^2 - {q_4}^2 & 2(q_2q_3 + q_1q_4) & 2(q_2q_4 - q_1q_3) \\ 2(q_2q_3 - q_1q_4) & {q_1}^2 + {q_3}^2 - {q_2}^2 - {q_4}^2 & 2(q_3q_4 + q_1q_2) \\ 2(q_2q_4 + q_1q_3) & 2(q_3q_4 - q_1q_2) & {q_1}^2 + {q_4}^2 - {q_2}^2 - {q_3}^2 \end{pmatrix} \begin{pmatrix} x \\ y \\ z \end{pmatrix} \tag{7}$$

Kearsley has shown[38] that rotation matrices that minimize the sum of the squared distances between corresponding atoms for two structures can be calculated posing a constrained least-squares problem in quaternion parameters. Posing: $x_- = x' - x$, $x_+ = x' + x$, with similar definitions for y_-, y_+, z_-, and z_+, the resulting equations can be organized in the eigenvalue problem shown below in eq 8.[36] In the elements of the 4×4 matrix of eq 8, the summation is made over the atoms to superimpose. Diagonalizing this symmetric matrix will give four orthogonal unit quaternions. The eigenvalues give the value of the residual for the rotation produced by application of the corresponding eigenvector. The rmsd is given by $(\lambda/n)^{1/2}$ where *n* is the number of atoms compared. The smallest eigenvalue gives the rotations that minimizes the sum of the distances between all corresponding atom.

5. Atomistic Simulations of Back Mapped Models

We want to stress that the proposed method for insertion of the atomistic details does not involve expensive potential energy and force evaluations. The adopted fully geometrical approach based on selection of the atomistic dihedrals from mesoscale angles and the successive structure superposition operates analytically and allows a very fast and efficient reconstruction of the atomistic model.

Just to have an idea, the reverse-mapping of the systems containing 150 chains of nine diads (corresponding to 150 10-mer chains, 24.750 atom positions were rebuilt), and three chains of 350 diads (corresponding 3 351-mer chains, 16.863 atom positions were rebuilt) took few seconds on a common personal computer (Pentium 4, 3 GHz).

The coordinates obtained from the reverse-mapping procedure described above have been minimized using harmonic positions restraints for methylene carbons. Furthermore, to avoid catenation between phenyl rings of different monomers, in the preparatory stage Lennard-Jones particles (phenyl centroids X) bounded to the atoms C1 and C4 of the phenyl ring (see Scheme 1) by rigid constraints have been added. Starting from scaled Lennard-Jones potentials (low values of ϵ and σ) in few hundreds of steepest descent minimization steps the nonbonded potential were brought linearly to their full values. At this stage, position restraints and phenyl centroids have been removed and, after short (1 ps) NVT MD equilibrations, NPT simulations have been run. In Figure 4 the mesocale and the reconstructed atomistic model of a 350-mer chain of atactic polystyrene are shown. The red beads are the meso and the yellow ones the racemo superatoms.

$$\begin{pmatrix} \sum({x_-}^2 + {y_-}^2 + {z_-}^2) & \sum(y_+z_- - y_-z_+) & \sum(x_-z_+ - x_+z_-) & \sum(x_+y_- - x_-y_+) \\ \sum(y_+z_- - y_-z_+) & \sum({x_-}^2 + {z_+}^2 + {y_+}^2) & \sum(x_-y_- - x_+y_+) & \sum(x_-z_- - x_+z_+) \\ \sum(x_-z_+ - x_+z_-) & \sum(x_-y_- - x_+y_+) & \sum({x_+}^2 + {z_+}^2 + {y_-}^2) & \sum(y_-z_- - y_+z_+) \\ \sum(x_+y_- - x_-y_+) & \sum(x_-z_- - x_+z_+) & \sum(y_-z_- - y_+z_+) & \sum({x_+}^2 + {y_+}^2 + {z_-}^2) \end{pmatrix} \begin{pmatrix} q_1 \\ q_2 \\ q_3 \\ q_4 \end{pmatrix} = \lambda \begin{pmatrix} q_1 \\ q_2 \\ q_3 \\ q_4 \end{pmatrix} \tag{8}$$

SCHEME 1: Atom Numbering for the All Atom Model of Polystyrene[a]

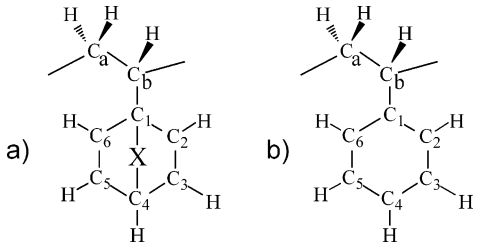

[a] (a) In the preparatory stage a centroid Lennard-Jones particle X is added to avoid ring catenation; (b) Model adopted in MD equilibration and production runs.

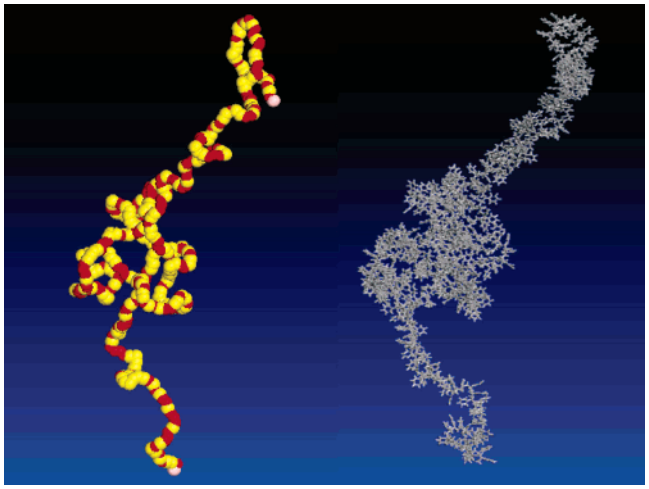

Figure 4. The mesocale and the reconstructed atomistic models of a 351-mer chains of atactic polystyrene. The red beads are the meso and the yellow ones the racemo superatoms.

To validate the reverse-mapping method proposed here, structural information obtained from atomistic simulations runs after reverse-mapping compared with available experimental data for atactic and syndiotactic polystyrene.

Radial distribution function obtained from wide-angle X-ray diffraction measurements on low molecular weight (0.79 kDa ~ monomers) atatic polystyrene has been reported by Londono et al.[37] In particular, they considered that, in atactic polystyrene, the dominant peaks in the total correlation functions are due to the two shortest carbon−carbon distances: aliphatic and aromatic. These are unimportant correlations which are almost independent of the molecular conformation and obscure the more important intermolecular components. Excluding C−C and C−C−C correlation components from their experimental data, they consider the remaining part of the total radial distribution function called $G_{rem}(r)$. In Figure 5 the experimental $G_{rem}(r)$ of atactic polystyrene and the one calculated from 1 ns of NPT MD simulation of 150 reverse-mapped decamers (1.0 kDa) are compared. The simulated and the experimental curves agree very well. A similar comparison between the data reported by Londono et. al has been made by Harmandaris et. al in ref 16.

High-molecular-weight atactic polystyrene X-ray structure factors (see Figure 6) are characterized by a diffuse halo (known as polymerization peak) at around $q = 7.5$ nm^{-1} in addition to a higher q feature at 14 nm^{-1} associated with an ubiquitous "amorphous halo" observed in polymer melts.[38]

To validate the ability of the proposed coarse grained model and the reverse-mapping method in the reproduction of the structure of polystyrene melts, X-ray scattering intensity calculated through Fourier transforms of the radial distribution

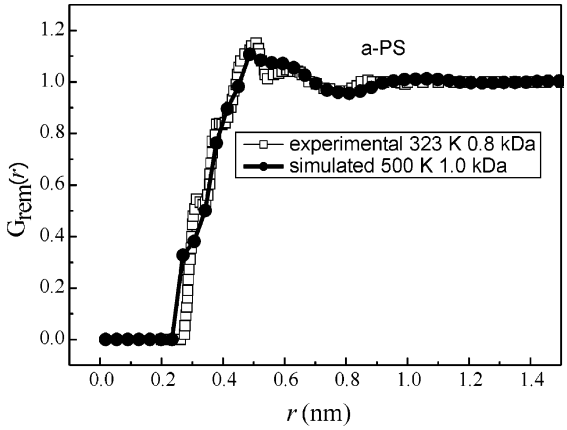

Figure 5. Carbons radial distribution function obtained from experiments (□) and from simulation of 150 back mapped 10-mer chains of atactic polystyrene (●).

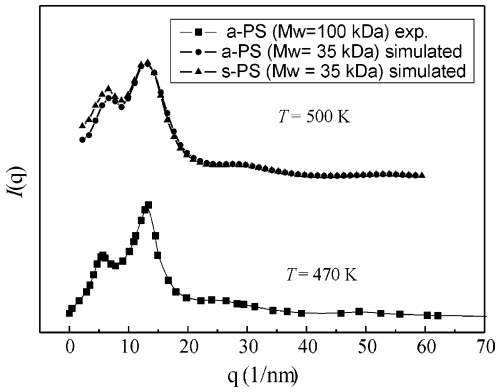

Figure 6. Experimental (atactic polystyrene, ■) and calculated X-ray diffraction profile for atactic (three chains of 351-mers, ●) and syndiotactic (three chains of 351-mers filled triangles) polystyrene.

functions obtained from back mapped atomistic models have been reported.

In Figure 6, the X-ray scattering profile calculated from 1 ns NPT MD simulation of three reverse-mapped chains of atactic polystyrene 351-mer (35 kDa) is reported together with the experimental curve. The experimental intensity pattern is well-reproduced by the simulated structures. As already reported in the literature, the amorphous halo arises primarily from phenyl−phenyl correlations, with important intramolecular and intermolecular contributions. The polymerization peak is due primarily to intermolecular correlations of backbone atoms. As a further test, analysis of dihedral conformations has been performed. The calculated value of trans conformer fraction $x_t = 0.6$ is in good agreement with solid-state NMR measurements[39] (x_t at 300 K in the range 0.58−0.78).

These results confirm the ability of coarse-grained model, and the relative reverse-mapping procedure, to take into account the structural features of specific polymers.

As reported above, the results of mesoscale simulations of syndiotactic chains are in good agreement with experimental findings in terms of coil dimension. In order to check the validity of the reverse-mapping procedure in the case of stereoregular polymer melts, the X-ray scattering intensity has been calculated from a 1 ns NPT MD simulation of three reverse-mapped chains of syndiotactic polystyrene 351-mer (35 kDa).

As reported by Guerra and co-workers[40] the diffraction patterns of quenched samples of syndiotactic and atactic polystyrene are very close. They differ in the height of the first peak (polymerization peak). In particular, the intensity of the

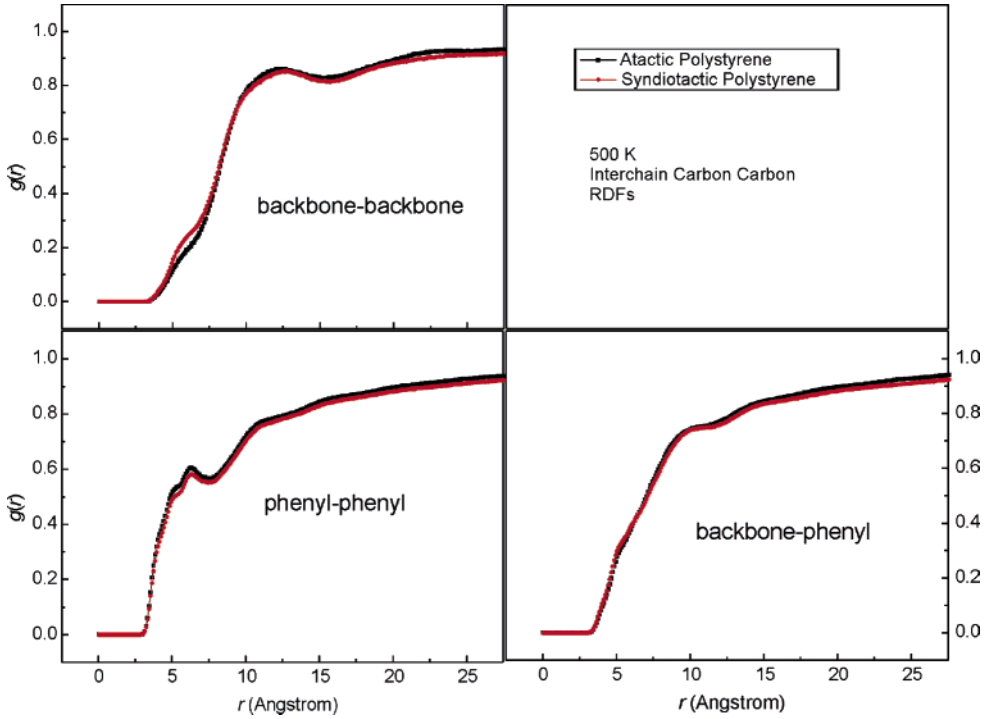

Figure 7. Interchain Carbons radial distribution functions (backbone−backbone, phenyl−backbone, phenyl−phenyl) from simulations of three back mapped 351-mer chains of atactic (black symbols) and syndiotactic polystyrene melts at 500 K.

polymerization peak is slightly higher in samples of syndiotactic polystyrene. This can be ascribed to a slight tendency of the syndiotactic polystyrene to chain alignment in the melt. From Figure 6 it is clear that the proposed coarse-grain model and the reverse-mapping method are able to reproduce even these small effects due to chain stereoregularity. The polymerization peak was found to be due primarily to intermolecular correlations of backbone atoms.[41] In Figure 7 interchain backbone−backbone, phenyl−backbone, and phenyl−phenyl carbons radial distribution functions from simulations of three back-mapped 351-mer chains of atactic (black symbols) and syndiotactic polystyrene melts are reported. The radial distribution functions of phenyl−backbone and phenyl−phenyl carbons of Figure 7 for atactic and syndiotactic chains are very close. The only small difference lies in the backbone−backbone correlation that results a bit higher for the syndiotactic chains between 4 and 8 Å.

Finally, we want to stress that, in the melt structures of high-molecular-weight atactic and syndioatctic polystyrene presented here (M_w of 35kDa), the chain length corresponds to at least 3 times the polystyrene entanglement length. As far as we know, this is the largest molecular weight of a polystyrene melt relaxed at atomistic level.

Conclusions

A systematic procedure to reintroduce atomistic degrees of freedom from coarse grain models of vinyl polymers has been developed and validated. The starting mesoscopic model consists of sequences of superatoms centered on methylene carbons of two different types according to the kind of diad (m or r) they belong to.

The proposed method is based on a fully geometrical approach and does not involve expensive potential energy and force evaluations. The selection of a suitable conformation of the dihedrals of the atomistic structure is based on the values of mesoscale angles. The successive structure superposition operated analytically allows a very fast and efficient reconstruction of the all atom model.

As a atomistic test case, all atom models of atactic and syndiotactic polystyrene have been obtained and successfully tested against experimental X-ray diffraction and solid-state NMR. The procedure proposed here allowed, for the first time, a relaxation at atomistic-level melts of atactic and syndiotactic polystyrene of molecular weight well beyond the entanglement length.

Acknowledgment. We are indebted to Prof. David Brown and Dr. Séverine Queyroy of Université de Savoie for providing the GMQ_num code. This work was partially supported by the MIUR of Italy (grants PRIN 2002 and FISR 1999), Università di Salerno (Fondo Medie Apparecchiature 2003), PODIME project (DL 297), and IMAST Scarl. We thank CINECA for allowing us CPU time (Progetti di Supercalcolo convenzione CINECA/INSTM). We thank Prof. Gaetano Guerra University of Salerno for useful discussions about syndiotactic polystyrene melt structure. We also thank Dr. Andrea Correa for helping us with the GROMACS program.

References and Notes

(1) Carmesin, I.; Kremer, K. *Macromolecules* **1988**, *21*, 2819.
(2) Paul, W.; Binder, K.; Kremer, K.; Heermann, D. *Macromolecules* **1991**, *24*, 6332.
(3) Baschnagel, J.; Binder, K.; Paul, W.; Laso, M.; Suter, U.; Batoulis, I.; Jilge, W.; Bürger, T. *J. Chem. Phys.* **1991**, *95*, 6014.
(4) Rapold, R.; Mattice, W. J. *Chem. Soc. Faraday Trans.* **1995**, *91*, 2435.
(5) Cho, J.; Mattice, W. *Macromolecules* **1997**, *30*, 637.
(6) Haliloğlu, T.; Mattice, W. *J. Chem. Phys.* **1998**, *16*, 6989.
(7) For a recent review see: Müller-Plathe, F. *ChemPhysChem* **2002**, *3*, 754.
(8) Reith, D.; Meyer, H.; Müller-Plathe, F. *Macromolecules* **2001**, *34*, 2335.
(9) Faller, R.; Müller-Plathe, F.; Doxastakis, M.; Theodorou, D. *Macromolecules* **2001**, *34*, 1436.
(10) Faller, R.; Kolb, A.; Müller-Plathe, F. *Phys. Chem. Chem. Phys.* **1999**, *1*, 2071.
(11) Faller, R.; Müller-Plathe, F.; Heuer, F. *Macromolecules* **2000**, *33*, 6602.

(12) Queyroy, S.; Neyertz, S.; Brown, D.; Müller-Plathe, F. *Macromolecules* **2004**, *37*, 7338.
(13) Milano, G.; Müller-Plathe, F. *J. Phys. Chem. B* **2005**, *109*, 18609.
(14) Sun, Q.; Faller, R. *Macromolecules* **2006**, *39*, 812.
(15) Sun, Q.; Faller, R. *J. Chem. Theory Comput.* **2006**, *2*, 607.
(16) Harmandaris, V. A.; Adhikari, N. P.; van der Vegt, N. F. A.; Kremer, K. *Macromolecules* **2006**, *39*, 6708.
(17) (a)Tschöp, W.; Kremer, K.; Han, O.; Batoulis, J.; Bürger, T. *Acta Polym.* **1998**, *49*, 75. (b) Queyroy, S.; Neyertz, S.; Brown, D.; Müller-Plathe, F. *Macromolecules* **2004**, *37*, 7338. (c) Hess, B.; Leon, S.; van der Vegt, N.; Kremer, K. *Soft Matter* **2006**, *2*, 409.
(18) Milano, G.; Goudeau, S.; Müller-Plathe, F. *J. Polym. Sci. Part B: Polym. Phys.* **2005**, *43*, 871.
(19) IUPAC Commission on Macromolecules Nomenclature, *Pure Appl. Chem.* **1979**, *51*, 1101; **1981**, *53*, 733.
(20) Berendsen, H. J. C.; van der Spoel, D.; van Drunen, R. *Comput. Phys. Commun.* **1995**, *91*, 43.
(21) Lindahl, E.; Hess, B.; van der Spoel, D. *J. Mol. Model.* **2001**, *7*, 306.
(22) Berendsen, H. J. C.; Postma, J.; van Gunsteren, W.; Di Nola, A.; Haak, J. *J. Chem. Phys.* **1984**, *81*, 3684.
(23) Allen, M. P.; Tildesley, D. J. *Computer Simulation of Liquids*; Clarendon Press: Oxford, 1987.
(24) Müller-Plathe, F. *Macromolecules* **1996**, *29*, 4782.
(25) Witt, R.; Sturz, L.; Dölle, A.; Müller-Plathe, F. *J. Phys. Chem. A* **2000**, *104*, 5716.
(26) Schmitz, H.; Müller-Plathe, F. *J. Chem. Phys.* **2000**, *112*, 1040.
(27) Milano, G.; Guerra, G.; Müller-Plathe, F.; *Chem. Mater.* **2002**, 2977
(28) Reith, D.; Pütz, M.; Müller-Plathe, F. *J. Comp. Chem.* **2003**, *24*, 1624.
(29) Queyroy S. Simulations moleculaires dynamiques de surfaces de polymeres amorphes: cas de la cellulose, Ph.D. Thesis, Universite de Savoie 2004.
(30) (a) Brown, D. The gmq User Manual Version 3, http://www.univ-savoie.fr/labos/lmops/brown/gmq.html. (b) Brown, D.; Minoux, H.; Maigret, B. *Comput. Phys. Commun.* **1997**, *103*, 170.
(31) Kenknight, C. E. *Acta Cryst.* **1984**, *A40*, 708.
(32) Honzatko, R. B. *Acta Cryst.* **1986**, *A42*, 172.
(33) Lesk, A. M. *Acta Cryst.* **1986**, *A42*, 110.
(34) Kearsley, S. K. *Acta Cryst.* **1989**, *A45*, 208.
(35) Weber, H. J.; Arfken, G. B. *Essential Mathematical Methods for Physicists*; Elsevier Academic Press: San Diego **2004**.
(36) Here, only the final formula useful for the purpose of this paper are reported. For complete proofs, see ref. 34.
(37) Londono, J. D.; Habenschuss, A.; Curro, J. G.; Rajasekaran, J. J. *J. Polym. Sci., Part B: Polym. Phys.* **1996**, *34*, 3055.
(38) Mitchell, G. R.; Windle, A. H. *Polymer* **1984**, *25*, 906.
(39) Dunbar, M. G.; Novak, B. M. Schmidt-Rohr, K. *Solid State NMR* **1998**, *12*, 119.
(40) Guerra, G.; Vitagliano, V. M; De Rosa, C.; Petraccone, V.; Corradini, P. *Macromolecules* **1990**, *23*, 1539.
(41) Ayyagari, C.; Bedrov, D.; Smith, G. D. *Macromolecules* **2000**, *33*, 6194.